Technical University of Denmark

DTU

The atomic structure of protons and hydrides in Sm1.92Ca0.08Sn2O7- pyrochlore from DFT calculations and FTIR spectroscopy

Bork, Nicolai Christian; Eurenius, K. E. J.; Rossmeisl, Jan; Knee, C. S.; Vegge, Tejs

DTU Library
Technical Information Center of Denmark

The atomic structure of protons and hydrides in Sm1.92Ca0.08Sn2O7−δ pyrochlore from DFT calculations and FTIR spectroscopy

N. Bork, K. E. J. Eurenius, J. Rossmeisl, C. S. Knee, and T. Vegge

Related Articles

Additional information on J. Appl. Phys.

The atomic structure of protons and hydrides in $Sm_{1.92}Ca_{0.08}Sn_2O_{7-\delta}$ pyrochlore from DFT calculations and FTIR spectroscopy

N. Bork,[1] K. E. J. Eurenius,[2] J. Rossmeisl,[3] C. S. Knee,[2] and T. Vegge[1,a)]

[1]*Department of Energy Conversion and Storage, Technical University of Denmark, 4000 Roskilde, Denmark*
[2]*Department of Chemistry, University of Gothenburg, SE-412 96 Göteborg, Sweden*
[3]*Center for Atomic-scale Materials Design, Department of Physics, Technical University of Denmark, DK-2800 Kgs. Lyngby, Denmark*

A combined density functional theory and Fourier transform infrared spectroscopy study of the structure and specific site preference of protons and hydrides in the pyrochlore $Sm_{1.92}Ca_{0.08}Sn_2O_{7-\delta}$ is presented. Two protonic sites of particular high stability are identified, both located on O(1) oxygen atoms closely associated with a Ca dopant. Further, the unexpected presence of H_O hydride defects in undoped, oxygen deficient $Sm_2Sn_2O_7$ is reported. Finally, the stretching frequencies and relative intensities for these and other sites are calculated. The main features of the Fourier transform infrared spectra are hereby resolved. © *2012 American Institute of Physics.* [http://dx.doi.org/10.1063/1.4737786]

I. INTRODUCTION

For many years, perovskites have been the benchmark system in the pursuit of oxide based proton conducting electrolytes.[1–4] Although extensively studied, no perovskite based material has obtained a sufficiently high protonic conductivity for commercial applications. Hence, interest has shifted to other structures. In spite of a large number of studies relating to high temperature oxide ion migration in $A_2B_2O_7$ pyrochlore systems,[5] there are relatively few studies of proton conduction at lower temperatures ($<550\,°C$).[4]

The pyrochlore structure has space group Fd-3m with Wyckoff positions 16(c) and 16(d) for the A and B metallic cations and 48(f) and 8(b) for the two structurally inequivalent oxygen atoms, denoted O(1) and O(2). The B cations are thus octahedrally coordinated by O(1) oxide ions while the A cations are tetrahedrally coordinated by O(2) oxide ions (see Fig. 1).[6,7] Pyrochlores thus contain a network of apex-linked BO_6 octahedra, which are expected to be critical for proton migration as found in perovskites.[7]

Investigations of high temperature proton conductivity in pyrochlores have so far been focused on acceptor doped derivatives of $Ln_2B_2O_7$, where $Ln =$ lanthanide and Y, and $B =$ Zr and Ti. The original work claiming significant proton conductivity in $La_2Zr_2O_7$ was performed by Shimura *et al.*[8] Subsequently, infrared (IR) spectroscopy,[9,10] electrochemical measurements,[11] and quantum mechanical simulations[7] have been performed to further investigate the proton mobility in the $La_2Zr_2O_7$ pyrochlore system. More recently, the influence of the B-site ion on proton conductivity in $Sm_{1.92}Ca_{0.08}B_2O_{7-\delta}$ phases ($B =$ Ti, Sn, Zr, and Ce) has also been studied,[12] and EMF measurements confirmed protons as the dominant charge carriers in $Sm_{1.92}Ca_{0.08}Ti_2O_{7-\delta}$ at T $\leq 400\ °C$.[13]

Several basic structural properties of protons in pyrochlores are still unresolved, and it is of interest to firmly establish the specific atomic configurations and protonic sites relevant for protonic diffusion. However, the specific protonic sites may be difficult to determine experimentally using, e.g., microscopy or x-rays.

In the last decades, *ab initio* calculations have become an attractive alternative due to the rapid increase in available computational power. The explicit atomic modelling provides direct insight into atomic interactions and configurations and a wide range of properties may be calculated, e.g., atomic structures and vibrational frequencies may be determined with good accuracy.[14]

In the present work, density functional theory (DFT) calculations and Fourier transform infrared spectroscopy (FTIR) data are combined to gain insight into the $Sm_{1.92}Ca_{0.08}Sn_2O_{7-\delta}$ structure at operating conditions. Using DFT, the Ca_{Sm} and V_O defective structure is determined, as well as the site preferences for the hydrogen/deuterium defect. Here, the Kröger-Vink notation scheme is used.[15] The results are confirmed by calculating the corresponding OH stretch vibrational frequencies and comparing with experimentally obtained FTIR spectra.

II. EXPERIMENTAL

$Sm_{1.92}Ca_{0.08}Sn_2O_{7-\delta}$ was prepared via conventional solid state synthesis from Sm_2O_3, $CaCO_3$, and SnO_2 at $1550\,°C$. Hydrogenation/deuteration was achieved by exposure to 0.4 bar gaseous H_2O/D_2O for 120 h at $300\,°C$.

The Fourier transform infrared (FTIR) measurements were performed in the range (560–6000 cm^{-1}). Each spectrum represents an average of 400 runs. A reference spectrum was measured on ground KBr before collecting each sample. For further details on the experiment, please refer to Eurenius *et al.*[16]

III. ELECTRONIC STRUCTURE CALCULATIONS

The calculations were performed using the VASP package using the projector augmented wave (PAW) method[17,18]

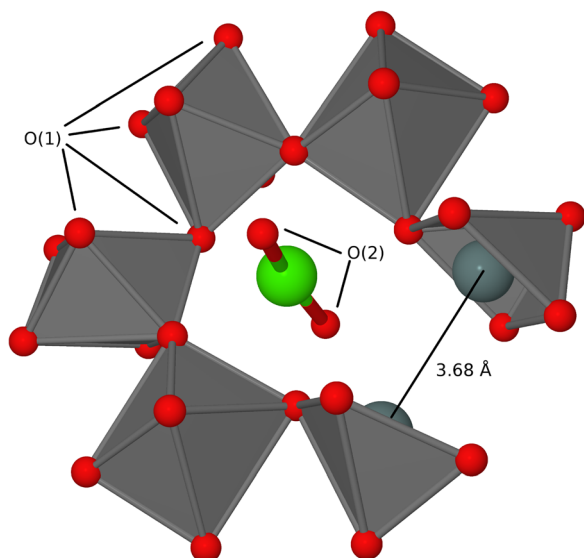a)Author to whom correspondence should be addressed. Electronic mail: teve@dtu.dk.

FIG. 1. Most stable configuration of the oxygen vacant $Sm_{1.875}Ca_{0.12}Sn_2O_{6.875}$. The structurally different O(1) and O(2) oxygen sites are indicated. The Sn-Sn distance around the oxygen vacancy is shortened to 3.68 Å compared to 3.73 Å in the defect free structure (Sm: omitted for clarity, Sn: grey, inside octahedra, Ca: green, O: red).

with exchange and correlation functionals by Perdew, Burke, and Entzerhof.[19] The Brillouin zone was sampled using a $2 \times 2 \times 2$ Monkhorst-Pack grid,[20] and the wavefunctions were determined via plane wavefunctions up to 400 eV. The electronic convergence criterion was 10^{-5} eV, and the force convergence criterion was 0.01 eV/Å. All super cells are charge neutral.

Having six 4f electrons, samarium is difficult to treat accurately with DFT. Here, we have used the PAW potential entitled "Sm_3", developed by Kresse and Joubert.[18] This is optimized for trivalent samarium by fixing five of the 4f electrons in the core while generating the pseudopotential. All of the 5s and 5p states are treated as valence states. Particularly concerning Lanthanides, the PAW description is superior to the also popular ultrasoft-pseudopotential approach[21] since the valence wavefunction in the core remains exact and hence favours the correct valence state and geometry.[22] Further, the PAW approach has repeatedly been successfully applied to compounds and alloys containing both Samarium and other Lanthanides.[22–24]

All internal degrees of freedom were relaxed during the ionic relaxations, but only the 5 oxygen atoms closest to the H defect were free to move in the vibrational analysis. Since restraining a part of the system could lead to inaccuracies, a test calculation with no constrained atoms was performed. The resulting constrained and non-constrained OH vibrational frequencies differed by less than one cm^{-1}, confirming the validity of this approach.

For determining atomic charges, the Bader charge partitioning method is applied.[25] This has proven suitable for OH containing systems in general and for hydrogen in oxides in particular, albeit requiring increased computational accuracy.[26–29] Therefore, the electronic convergence criterion was decreased to 10^{-7} eV for obtaining high accuracy electronic densities via expanding the wavefunctions and the

localized charges on $300 \times 300 \times 300$ and $450 \times 450 \times 450$ real-space uniform grids, respectively. The algorithm by Henkelman *et al.* was used for the actual charge partitioning.[29–31]

IV. RESULTS AND DISCUSSION

A. Thermodynamics

The Gibbs free energy change of a chemical reaction is in the dilute limit given by

$$\Delta G = \Delta E - T\Delta S, \qquad (1)$$

where ΔE denotes the internal energy, T denotes the temperature, and ΔS denotes the entropy change. Several corrections to known inaccuracies of DFT may be employed. Here we only correct for the known overbinding of O_2.[7] Further corrections, e.g., for Fermi level inaccuracies or electronic correlation could be employed but are non-trivial and beyond the objective of this study.

The unit cell of $Sm_2Sn_2O_7$ contains 8 chemical units (88 atoms) so the experimentally obtained starting composition ($Sm_{1.92}Ca_{0.08}Sn_2O_{6.96}$) was modelled by inclusion of one Ca_{Sm} dopant and one oxygen vacancy, yielding $Sm_{1.875}Ca_{0.125}Sn_2O_{6.875}$. This size cell has previously been found to be a good compromise between accuracy and computational expense.[7] Given the fixed doping concentration of the synthesized material, any interlattice defect interactions are intended and desired.

Initially, the cubic unit cell constant was optimized to 10.536 Å in good agreement with previous experiments (10.514 Å).[16] The relative vacancy formation energies of O(1) and O(2) defects were determined to ca. 160 kJ/mol favoring $V_{O(1)}$ vacancies. The most stable $V_{O(1)}$ vacancy, shown in Fig. 1, is used as reference structure for the remaining of this article. This is stabilized by 16 kJ/mol compared to the second most stable $V_{O(1)}$ site.

Given an oxygen deficient structure, incorporation of protons is known to proceed via filling of oxygen vacancies by water[3]

$$H_2O(g) + V_O^{\bullet\bullet} + O_O^x \leftrightarrow 2\ OH_O^\bullet. \qquad (2)$$
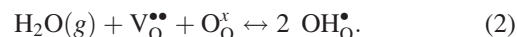
The stabilities of 20 different protonic sites were investigated. All of the most stable sites were found closely associated with a Ca_{Sm} dopant. When formed via reaction (2), these were stabilized by up to 137 kJ/mol H, in reasonable accordance with experimental data of ca. 100 kJ/mol.[16] Similar thermodynamics were found by Björketun *et al.* in the case of Ca doped $La_2Zr_2O_7$ pyrochlore.[7] As mentioned above, prediction of absolute defect formation energies is difficult and a variety of correctional schemes may be employed for increased accuracy. However, the energy gain of reaction (2) is so high that full occupation of the oxygen vacancies should be achieved under working membrane conditions. Since both theory and experiments suggest highly negative OH formation energies, the reported incomplete (72%) hydration of the oxygen vacancies, based on thermogravimetric analyses,[32] is most likely due to migration of

Ca_{Sm} dopants into grain boundaries or to kinetic limitations in the experiment.

The two most stable sites for the hydrogenic defect were bonded to structurally identical oxygen, O(1), located at the former oxygen vacancy sites. These two $OH_{O(1)}$ defects differ by the spatial orientation of the OH bond and differ in stability by just 2.3 kJ/mol. The H-Ca distances are 2.48 and 4.14 Å. Two other sites of interest were identified, destabilized by ca. 18 kJ/mol, and distanced by 4.70 and 5.59 Å from the dopant. These four sites are shown in Fig. 2.

At elevated temperatures, protons may migrate to sites near oxygen vacancies. Here, we only consider the most stable $V_{O(1)}$ containing structure, shown in Fig. 1. 10 different protonic sites were investigated, and two sites of particular low energy were found. These were both bound to an O(1) atom neighbouring the $V_{O(1)}$ vacancy but differed in the spatial orientation of the OH bond (see Fig. 3). These structures were however >150 kJ/mol less stable than the corresponding oxygen stoichiometric structures.

Also the structure of hydrogenated, non-doped, but oxygen deficient $Sm_2Sn_2O_7$ was determined. In the most stable structure, the proton was found not as a hydroxyl but located at the oxygen vacancy as an $H_O^{\bullet}$ defect (see Fig. 4). This is in accordance with previous assumptions and recent *ab initio* calculations.[33,34] Formally, $H_O^{\bullet}$ is a hydride and thus, similar to an oxide, has two valence electrons and an ionic radius of ca. 1.4 Å. Also similar to oxides, the incorporation of hydride defects requires electrons, which in this case must be donated from the remaining lattice atoms

$$H_2(g) + 2\ V_O^{\bullet\bullet} + 2\ e' \leftrightarrow 2\ H_O^{\bullet}. \qquad (3)$$
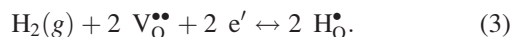
Even disregarding entropy, the defect formation energy corresponding to this reaction was >100 kJ/mol favoring gase-

FIG. 3. Most stable (white H) and second most stable (yellow H) configuration of a proton and an oxygen vacancy in $Sm_{1.875}Ca_{0.125}Sn_2O_7$ (Sm and O(2): omitted for clarity, Sn: inside octahedra, Ca: green, O(1): red, H: white and yellow).

ous hydrogen. Hence, it is evident that the expected H_O defect concentration is very low at ambient conditions. Its general properties and state of charge are nevertheless of fundamental interest and are further described in the following section.

At moderate temperatures, structural dopants are prerequisites for oxygen vacancies and hence dissolved protons via reaction (2), but dopants are also known to act as trapping sites preventing fast diffusion.[35,36] From these results, it is clear that also in this system, significant trapping effects may be present if too low dopant concentrations are used, i.e., if the proton has to diffuse through effectively undoped regions between dopants. Due to the presence of several low energy sites at varying distance from the dopant, as shown in Fig. 2,
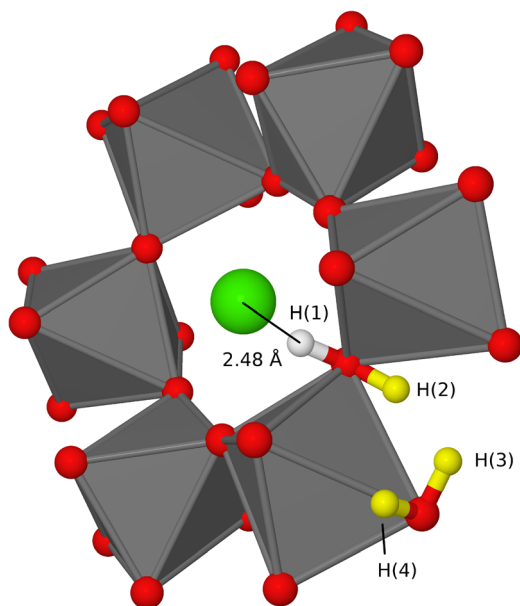

FIG. 2. Most stable configuration (white H) of a proton in $Sm_{1.875}Ca_{0.125}Sn_2O_7$. The Ca-H distance is 2.48 Å and the Ca-O-H angle is ca. 63°. The yellow hydrogen are included to illustrate the three second most stable sites (Sm and O(2): omitted for clarity, Sn: inside octahedra, Ca: green, O(1): Red, H: white and yellow).
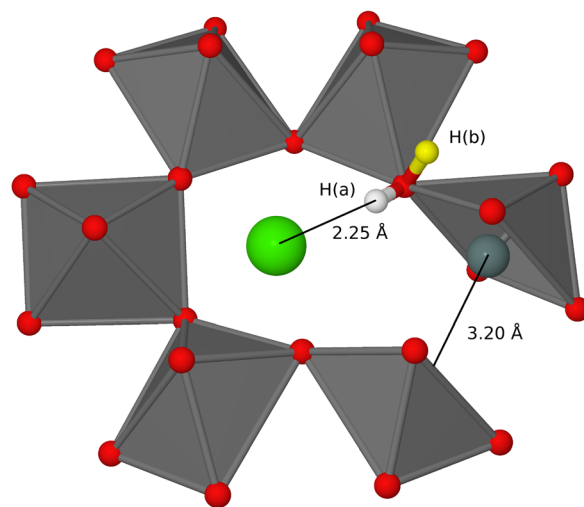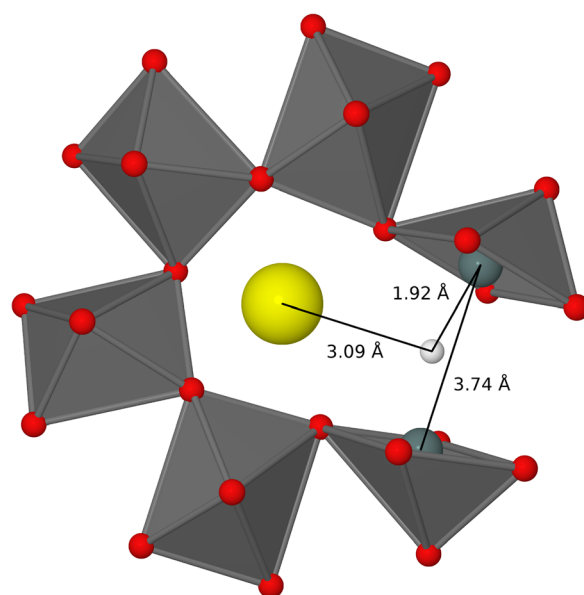

FIG. 4. Most stable configuration of a proton and an oxygen vacancy in $Sm_2Sn_2O_7$. The Sn-H distance is 1.9 Å while normal Sn-O distances are 2.1 Å. The charge on the H_O species is −0.44e (Sm: yellow, Sn: grey (inside octahedra), O(1): red, O(2): omitted for clarity, H: white).

TABLE I. Summary of the atomic Bader charges (in e). The charges predicted by traditional defect chemistry are listed for comparison.

Defect structure	Fig.	Ca_{Sm}	V_O	OH_O	H_O
Trad. def. chem.		−1.00	2.00	1.00	1.00
$Ca_{Sm}V_O$	1	−0.56	1.26		
$Ca_{Sm}OH(1)_O$	2	−0.56		0.57	
$Ca_{Sm}V_OOH(a)_O$	3	−0.59	1.26	0.55	
Undoped H_O	4				0.82

a path of low energy sites between dopants is available if one dopant is present in each unit cell. However, a full kinetic analysis of the trapping effects of dopants is beyond the scope of this study.

B. Atomic charge distributions

To analyse and predict possible multiple defect configurations, electrostatic defect interaction is the most important parameter since all present defects are electrically charged. It is generally assumed that oppositely charged defects attract while defects of similar charge repel each other. Recently, it has however been demonstrated that elastic lattice interactions can stabilize otherwise unstable configurations.[37]

To explain the configurations of the most stable structures, shown in Figs. 1–4, these were investigated using the Bader charge partitioning method. The results are summarized in Table I. The determined atomic charges are not integers and smaller in magnitude than the integer charges predicted by traditional defect chemistry. The signs are however unchanged.

It is thus possible to assign the attractive interaction between the Ca_{Sm} dopant and either of the V_O or the OH_O defects (Figs. 1 and 2) mainly to Coulomb attraction. However, since the total charge of the $Ca_{Sm}V_O$ defect ($0.67e$) is of same sign and magnitude as the OH_O defect, it is not immediately clear why the proton is attracted rather than repelled by the $Ca_{Sm}V_O$ defect (Fig. 3). However, the stabil-

ity of two OH_O defects in oxides has recently been demonstrated and explained by elastic lattice interaction, minimizing lattice distortion by gathering defects.[37,38] The overall attractive force between the $Ca_{Sm}V_O$ and OH_O defects is thus proposed to be due to this effect.

The H_O defect has been proposed as a possible hydride site, responsible for the observed hydride conductivity in some oxides.[39–42] The apparent hydride conductivity has only been observed under highly reducing conditions and high temperatures; both conditions promoting high V_O concentration and mobility. This is consistent with the H_O defect being the charge carrier. Here, the integrated electronic density on the H_O defect was determined to 1.44 electrons and the total charge thus $−0.44e$. Hence, the charge of the hydride is similar in magnitude to the charge designated to the proton. However, since the hydride is located at an oxygen vacancy, $V_O^{1.26\bullet}$, the defect is positive and should be referred to as $H_O^{0.82\bullet}$.

C. Vibrational frequencies

From the experimentally obtained FTIR spectra several distinct peaks were identified, confirming the presence of dissolved protons in the structure (see Fig. 5). The two most intense peaks show clear isotopic shifts with isotopic shift ratios, $\nu_{OH}/\nu_{OD} \sim 1.35$, referring to the change in mass between O-H and O-D groups in accordance with the expected value.[43] Similar to the main O-H peak, the main O-D peak has at least one shoulder. However, this is probably the phonon overtone at ca. $2540\,cm^{-1}$, seen in the vacuum dried sample. The minor peaks at 2615 and $3510\,cm^{-1}$ are also phonon overtones not linked to structural protons or deuterons.

The protonated spectrum was resolved using Lorentzian functions

$$\mathcal{L}(\nu) = \mathcal{A}\frac{1}{\pi}\frac{\frac{1}{2}\mathcal{B}}{(\nu - \nu_0)^2 + (\frac{1}{2}\mathcal{B})^2}, \quad (4)$$

where $\mathcal{A}$ and $\mathcal{B}$ are parameters determining the height and width of the peak, centered at ν_0. Using four Lorentzians centered at 3311, 3387, 3422, and $3454\,cm^{-1}$, a near-perfect fit was obtained. Since the areas of the peaks, $\mathcal{A}$, are proportional to the occupancies of the OH sites,[44] these were hereafter readily available (see Table II).

FIG. 5. FTIR spectra of protonated and deuterated $Sm_{1.92}Ca_{0.08}Sn_2O_{7−\delta}$ (solid lines). $*$ indicates frequencies not linked to O-H/O-D vibrations. Vacuum dried samples are shown for comparison (broken lines). The ratios between the corresponding OH and OD frequencies are, as expected, close to 1.35. Data from Ref. 14.

TABLE II. Calculated and experimental intensities at 300 °C and OH stretch frequencies (in cm^{-1}) of the most stable proton sites, relative to the main peak. The H(1-4) sites are illustrated in Fig. 2.

Defect structure	DFT		FTIR	
	Intens.	Wavenum.	Intens.	Wavenum.
$Ca_{Sm}OH(1)_O$	100%	3453	100%	3454
$Ca_{Sm}OH(2)_O$	59%	3312	72%	3311
$Ca_{Sm}OH(3)_O$	5%	3252		
$Ca_{Sm}OH(4)_O$	3%	3321		
Undoped OH_O	~0	3340		
Undoped H_O	~0	3280		

The vibrational frequencies depend on the second derivative of the energy and are inherently more difficult to calculate than, e.g., simple energy differences. Consequently, absolute agreement between DFT and FTIR results is seldom achieved. Typically, GGA functionals overestimate bond lengths and underestimate frequencies,[45] but although unable to produce accurate absolute numbers, trends and shifts generally are good.[46–48]

To quantify this problem, frequency calculations on gaseous H_2O and H_2O_2 were performed and compared to experimental values.[49,50] With the present computational parameters, the calculated OH stretch frequencies were all overestimated by 50–90 cm^{-1}. This suggests that the calculated OH frequencies for the present systems should be adjusted accordingly. By adjusting the calculated frequencies by -80 cm^{-1} an excellent agreement between theory and experiment was obtained, both with respect to wavenumbers and intensities (see Table II). The two most intense peaks, at 3454 and 3311 cm^{-1}, are thus unambiguously assigned to OH vibration from the OH(1) and OH(2) sites, respectively, both shown in Fig. 2.

Earlier studies by Omata *et al.*,[9,10] showing three bands in the OH frequency region in protonated $La_{1.96}Ca_{0.04}Zr_2O_{7-\delta}$, assigned one of the intense bands to protons bound to O(2) oxygen. This was based on empirical relations between O-H and O-O distances and O-H wavenumbers.[51] Our results show that a proton at the O(2) site is destabilized by ca. 60 kJ/mol compared to the most stable $OH_{O(1)}$ site. This is in agreement with the findings of Björketun *et al.* for $La_2Zr_2O_7$.[7] The $OH_{O(2)}$ defect is thus insignificantly populated at ambient temperatures.

We were unable to identify the shoulders at 3387 and 3422 cm^{-1} with certainty, although the H(4) site is a possible candidate. Otherwise, these shoulders may be attributed to structures involving a different $V_{O(1)}$ than shown in Fig. 1 or structures involving more than two defects, e.g., two Ca dopants and a proton or two protons and a Ca dopant.[7,37]

V. CONCLUSIONS

Using density functional theory calculations and Fourier transform infrared spectroscopy, as-prepared, protonated, and deuterated samples of $Sm_{1.92}Ca_{0.08}Sn_2O_{7-\delta}$ pyrochlore were investigated. In the most stable configuration, the V_O defect was located on an O(1) site next to the Ca_{Sm} dopant. Two protonic sites of particular low energy were found, whereby the magnitudes and intensities of the main bands of the FTIR spectrum could be reproduced with high certainty.

To explain the attractive potentials between the various defects, their atomic charges were determined. Hereby, the stability of all structures could be rationalized. In accordance with previous results,[37] the OH_O defect was found to be charged by ca. 0.55e. We also report the finding of an H_O defective oxide structure and determine this defect as a hydride.

ACKNOWLEDGMENTS

[1]H. Iwahara, Solid State Ionics **77**, 289 (1995).
[2]R. C. T. Slade, Solid State Ionics **61**, 111 (1993).
[3]K. D. Kreuer, E. Schönherr, and J. Maier, Solid State Ionics **70–71**, 278 (1994).
[4]N. Bork, N. Bonanos, J. Rossmeisl, and T. Vegge, Phys. Rev. B **82**, 014103 (2010).
[5]S. A. Kramer and H. L. Tuller, Solid State Ionics **82**, 15 (1995).
[6]E. J. Harvey, K. R. Whittle, G. R. Lumpkin, R. I. Smith, and S. A. T. Redfern, J. Solid State Chem. **178**, 800 (2005).
[7]M. E. Björketun, C. S. Knee, B. J. Nyman, and G. Wahnström, Solid State Ionics **178**, 1642 (2008).
[8]T. Shimura, M. Komori, and H. Iwahara, Solid State Ionics **86–88**, 685 (1996).
[9]T. Omata, M. Tagaki, and S. Otsuka-Matsuo-Yao, J. Electrochem. Soc. **150**, E590 (2003).
[10]T. Omata and S. Otsuka-Matsuo-Yao, J. Electrochem. Soc. **148**, E475 (2001).
[11]T. Omata and S. Otsuka-Yao-Matsuo, J. Electrochem. Soc. **148**, E252 (2001).
[12]K. E. J. Eurenius, E. Ahlberg, and C. S. Knee, Dalton Trans. **40**, 3946 (2011).
[13]K. E. J. Eurenius, H. K. Bentzer, N. Bonanos, E. Ahlberg, and C. S. Knee, J. Solid State Electrochem. **15**, 2571 (2011).
[14]F. Jensen, *Introduction to Computational Chemistry* (Wiley, New York, 1999).
[15]F. Kröger and H. Vink, Solid State Phys. **3**, 301 (1956).
[16]K. E. J. Eurenius, E. Ahlberg, and C. S. Knee, Solid State Ionics **181**, 1577–1585 (2010).
[17]P. E. Blöchl, Phys. Rev. B **50**, 17953 (1994).
[18]G. Kresse and D. Joubert, Phys. Rev. B **59**, 1758 (1999).
[19]J. P. Perdew, K. Burke, and M. Ernzerhof, Phys. Rev. Lett. **77**, 3865 (1996).
[20]H. J. Monkhorst and J. D. Pack, Phys. Rev. B **13**, 5188 (1976).
[21]D. Vanderbilt, Phys. Rev. B **41**, 7892 (1990).
[22]N. Hirosaki, S. Ogata, and C. Kocer, J. Alloy Compd. **351**, 31–34 (2003).
[23]A. Ismail, J. Hooper, J. B. Giorgi, and T. K. Woo, Phys. Chem. Chem. Phys. **13**, 6116–6124 (2011).
[24]W. Chen, P. Yuan, S. Zhang, Q. Sun, E. Liang, and Y. Jia, Physica B **407**, 1038–1043 (2012).
[25]R. F. W. Bader, Can. J. Chem. **76**, 973–988 (1998).
[26]N. Bork, T. Kurtén, M. B. Enghoff, J. O. P. Pedersen, K. V. Mikkelsen, and H. Svensmark, Atmos. Chem. Phys. **11**, 7133–7142 (2011).
[27]N. Bork, T. Kurtén, M. B. Enghoff, J. O. P. Pedersen, K. V. Mikkelsen, and H. Svensmark, Atmos. Chem. Phys. Discussions **11**, 29647–29679 (2011).
[28]N. Bork, N. Bonanos, J. Rossmeisl, and T. Vegge, J. Appl. Phys. **109**, 033702 (2011).
[29]G. Henkelman, A. Arnaldsson, and H. Jónsson, Comp. Mater. Sci. **36**, 3 (2006).
[30]E. Sanville, S. D. Kenny, R. Smith, and G. Henkelman, J. Comput. Chem. **28**, 5 (2007).
[31]W. Tang, E. Sanville, and G. Henkelman, J. Phys.-Condens. Mater. **21**, 084204 (2009).
[32]K. E. J. Eurenius, E. Ahlberg, I. Ahmed, S. G. Eriksson, and C. S. Knee, Solid State Ionics **181**, 148 (2010).
[33]Y. Iwazaki, T. Suzuki, and S. Tsuneyuki, J. Appl. Phys. **108**, 083705 (2010).
[34]T. Norby, M. Widerøe, R. Glöckner, and Y. Larring, Dalton Trans. 3012–3018 (2004).
[35]J. Voss, Q. Shi, H. S. Jacobsen, M. Zamponi, K. Lefmann, and T. Vegge, J. Phys. Chem. B **111**, 3886–3892 (2007).

[36]M. E. Björketun, P. G. Sundell, and G. Wahnström, Phys. Rev. B **76**, 054307 (2007).

[37]N. Bork, N. Bonanos, J. Rossmeisl, and T. Vegge, Phys. Chem. Chem. Phys. **13**, 15256 (2011).

[38]M. C. Tarun and M. D. McCluskey, J. Appl. Phys. **109**, 063706 (2011).

[39]M. Widerøe, N. Kochetova, and T. Norby, Dalton Trans. **19**, 3147 (2004).

[40]M. Widerøe, R. Waser, and T. Norby, Solid State Ionics **177**, 1469–1476 (2006).

[41]S. Steinsvik, Y. Larring, and T. Norby, Solid State Ionics **143**, 103 (2001).

[42]T. Norby and Y. Larring, Solid State Ionics **136–137**, 139–148 (2000).

[43]M. J. Wojcik, J. Lindgren, and J. Tegenfeldt, Chem. Phys. Lett. **99**, 112 (1983).

[44]B. Andes Hess, Jr., L. J. Schaad, P. Carsky, and R. Zahradnik, Chem. Rev. **86**, 709 (1986).

[45]C. Adamo, M. Ernzerhof, and G. E. Scuseria, J. Chem. Phys. **112**, 2643 (2000).

[46]J. O. Jensen, Spectrochim. Acta A **58**, 1347–1364 (2002).

[47]R. G. Parr and W. Yang, *Density Functional Theory of Atoms and Molecules* (Oxford Univ. Press, Oxford, 2002).

[48]M. Karlsson, M. E. Björketun, P. G. Sundell, A. Matic, G. Wahnström, D. Engberg, L. Börjesson, I. Ahmed, S. Eriksson, and P. Berastegui, Phys. Rev. B **72**, 094303 (2005).

[49]J. D. Cox, D. D. Wagman, and V. A. Medvedev, *CODATA Key Values for Thermodynamics* (Hemisphere, New York, 1989).

[50]T. Shimanouchi, J. Phys. Chem. Ref. Data **6**, 993 (1977).

[51]A. Novak, Struct. Bonding **18**, 177 (1974).